Chapter 9

Robustness of finger-vein recognition

Christof Kauba[1] and Andreas Uhl[1]

9.1 Introduction

One of the big issues in biometric recognition is robustness of recognition accuracy against sample signal quality degradation. The performance of a biometric recognition system is usually heavily affected by sample signal quality. A wide variety of factors potentially influence the quality of acquired biometric samples.

The different types of features that can be extracted from biometric samples influence the impact of quality degradations on recognition performance in various ways. Moreover, there is interplay among different types of feature extraction and acquisition technology/conditions such that it is not clear a priori which type of feature extraction is favourable under which conditions. Therefore, it is essential to provide reliable methodology to comparatively assess biometric recognition robustness under varying conditions.

Fingerprint recognition is a prominent biometric field in which robustness of recognition accuracy against sample image quality degradation is a central issue [1,2]. The quality of fingerprint images is influenced by skin conditions (e.g. dryness, moisture, dirt, age, cuts, and bruises), sensor conditions (e.g. dirt, noise, and size), and other acquisition conditions like user cooperation or crime scene preservation in forensic settings, etc. Some of these factors are inevitable, and some of them change over time. Poor quality images often result in spurious and missed features, therefore decreasing the recognition accuracy of the overall system.

In fingerprint recognition, this issue is classically tackled from two sides: First, benchmarking frameworks have been established, which facilitate a common evaluation basis with standardised protocols for various fingerprint recognition algorithms, see e.g. the fingerprint verification contests (FVC [2]) as well as independent suggestions like [3] and the BioSecure evaluation framework [1]. Second, usually these frameworks rely on the establishment of test data which are used to compare the different algorithms on a common basis. A very good example, specifically focusing onto the robustness issue, is the FVC datasets. FVC2002 (only (i) and (iv)) and FVC2004 data have been acquired in a way to introduce higher

[1]Department of Computer Sciences, University of Salzburg, Austria

intra-class variation by (i) putting the finger at slightly different vertical position, (ii) applying low or high pressure against the sensor, (iii) exaggerating skin distortion and rotation, and (iv) drying or moistening fingers. For FVC2006, the population was chosen to be more heterogeneous, including manual workers and elderly people.

While the availability of these and similar datasets is a significant achievement, the data collection and database establishment are tedious works. Moreover, if additional acquisition conditions should be considered which have not been included into the original dataset, re-enrolment is required, involving complicated procedures for getting the original people back to enrolment. Also, it is hard to compare the different quality degradations from dataset to dataset (e.g. FVC, MCYT, BIOMET, and MSU), since usually, there is no standardised manner to generate the acquisition conditions applied. Therefore, the experimental results of recognition algorithms in case applied to different datasets are hardly comparable, and the results shown in many papers are difficult to interpret.

A strategy to cope with the various problems of generating natural datasets is to generate synthetic fingerprints, the SFinGe [4] being the most well-known tool for doing this. The generated fingerprints have proven to be highly realistic and serve as a sensible tool to generate large datasets for benchmarking. While SFinGe also allows to apply some manipulations to the images, e.g. noise insertion, translations, rotations, and uses a skin deformation model, a simulation of specific sensor types is not foreseen. In related work, we have proposed the watermarking robustness assessment toolkit *StirMark* [5] to be used as standardised tool in fingerprint recognition robustness assessment [6,7], which is able to simulate a wide class of acquisition conditions, applicable to any given (natural) dataset. We have also applied a simulation of sensor ageing to natural image datasets to assess sensor ageing robustness of fingerprint recognition systems [8].

However, for hand- and finger-vein recognition systems, there are neither natural benchmark datasets focussing on robustness issues nor corresponding robustness evaluation results available. Also, robustness evaluations on simulated datasets are limited to our own previous work on

- hand-vein recognition, where we assess
  - the impact of simulated sensor ageing and StirMark-based distortions on the recognition performance of hand-vein recognition [9], and
- finger-vein recognition, where we assess
  - the impact of simulated sensor ageing [10] and
  - the impact of ISO lossy compression standards on the recognition performance of finger-vein recognition [11].

For finger-vein recognition, the data available so far on sensor ageing and compression robustness [10,11] is restricted to a single dataset only (with unknown generalisation to different datasets/sensors), and for compression robustness assessment, results only include equal error rate (EER) data and a single compression scenario (both probe and gallery compressed). StirMark-based distortions, simulating various acquisition conditions, have not yet been investigated for their impact on this modality at all. We will tackle these issues by providing more

complete experimental results to provide a better understanding of finger-vein recognition techniques' robustness in this chapter.

In Section 9.2, we describe the finger-vein recognition algorithms applied and the datasets used. Section 9.3 deals with the simulation of varying acquisition conditions using the StirMark toolkit and corresponding impact on recognition accuracy. In Section 9.4, we describe the impact of applying four different lossy compression algorithms on recognition discriminating two different application scenarios. Section 9.5 presents results on sensor-ageing robustness considering artificially aged datasets. Finally, Section 9.6 concludes this chapter.

9.2 Finger-vein recognition and datasets

9.2.1 Finger-vein recognition algorithms

Pre-processing can be grouped into methods to align the finger position and to improve the low contrast and image quality. For finger alignment, we use a method adopted from Lee *et al.* [12] (**LeeRegion**) which simply masks out background pixels (setting them to 0). This is followed by a **normalisation** step, i.e. rotation compensation as done in [13].

For image enhancement, we apply Contrast Limited Adaptive Histogram Equalisation (CLAHE) [14] as the final stage of **high frequency emphasis (HFE) filtering** which was originally proposed for hand vein image enhancement [15]. Also, CLAHE is used to post-process a filtering using a **Circular Gabor Filter** (**CGF**) as proposed by Zhang and Yang [16].

To foster reproducible research, we have only included *feature extraction* techniques in this study for which basic implementations are available as open-source software. The first scheme discussed aims to extract the vein pattern from the background resulting in a binary image, followed by a comparison of these binary images using a correlation measure.

Maximum curvature (MC [17]) aims to emphasise only the centre lines of the veins and is therefore insensitive to varying vein width. The first step is the extraction of the centre positions of the veins. Therefore, the local MC in the cross-sectional profiles, based on the first and second derivatives, is determined. Afterwards, each profile is classified as being concave or convex where only local maxima in concave profiles indicate valid centre positions of the veins. Then a score according to the width and curvature of the vein region is assigned to each centre position, which is recorded in a matrix called locus space. Due to noise or other distortions, some pixels may not have been classified correctly at the first step; thus the centre positions of the veins are connected using a filtering operation. Finally, binarisation is done by thresholding using the median of the locus space.

For matching the binary feature images, we adopted the approach in [17,18]. As the input images are not registered to each other and only coarsely aligned (rotation is compensated), the correlation between the input image and in x- and y-direction shifted versions of the reference image is calculated. The maximum of these correlation values is normalised and then used as final matching score.

In contrast to MC, the Scale Invariant Feature Transform (SIFT) keypoint [19] based technique uses information from the most discriminative points as well as considering the neighbourhood and context information of these points by extracting key points and assigning a descriptor to each key point. We employ an additional key point filtering as described in [20], where keypoints close to the finger/background boundary are discarded in addition to eventual background keypoints.

SIFT matching is done using the keypoint descriptors – the keypoint with the smallest distance to the reference keypoint is the matched one if the distance is below a threshold, otherwise there is no match. To resolve the problem with ambiguous matches (i.e. one keypoint may have small distances to more than one other point), the classical ratio threshold scheme is used: A match is only valid if the distance of the best point match is at least k (threshold) times smaller than to all other points.

For MC, LeeRegion, Normalisation, and CGF pre-processing has been applied (MC software of B.T. Ton[1] is used), while for SIFT feature extraction, LeeRegion, Resize, CGF, and HFE pre-processing has been used (SIFT feature extraction and matching software is used as provided by VL_Feat SIFT[2]). For more details on the used pre-processing and feature-extraction methods, the interested readers are referred to [20].

9.2.2 Datasets

For experimental evaluations in this chapter, we use the following two publicly available finger-vein datasets:

- **UTFVP**: University of Twente Finger Vascular Pattern (UTFVP) Database [21], consisting of a total of 1,440 images, taken from 60 subjects, 6 fingers per subject and 4 images per finger. The images have a resolution of 672 × 380 pixel with 8-b greyscale depth.
- **SDUMLA-HMT**: This multi-modal dataset was collected during the summer of 2010 at Shandong University, Jinan, China. 106 subjects, including 61 males and 45 females with age between 17 and 31, participated in the data-collecting process, in which all the five biometric traits – face, finger vein, gait, iris, and fingerprint are collected for each subject [22]. SDUMLA-HMT is available at http://mla.sdu.edu.cn/sdumla-hmt.html. The finger-vein dataset consists of 6 fingers per subject, 6 images per finger, 3,816 images, 320 × 240 pixel with 8-b grey level.

The test procedure of the FVC2004 [23] was adopted to determine the EER. For the genuine matches (to determine False Non-Match Rate (FNMR)), each image of each finger is compared with all remaining images of the same finger, no symmetric matches are performed. For the impostor matches (to determine False Match Rate (FMR)), the first image of each finger is compared against the corresponding first image of the same finger of all remaining subjects, again no symmetric matches are performed.

[1]Publicly available on MATLAB Central: http://www.mathworks.nl/matlabcentral/fileexchange/authors/57311.
[2]http://www.vlfeat.org/.

9.3 StirMark distortion robustness: modelling acquisition conditions

Petitcolas *et al.* [24] developed a benchmark test in the context of robustness evaluation for digital image watermarking methods, called StirMark.[3] The basic idea behind their benchmark test is that a digital watermark embedded inside an image can be attacked by introducing different small image manipulations to the watermarked image. The specific types of perturbations are pre-defined, and their intensity can be adjusted via a given set of parameters for each type of perturbation.

Utilising StirMark to generate datasets for robustness evaluations has several advantages. First of all, the tests are reproducible if their parameters are known and the test dataset is available. Moreover, it is possible to systematically simulate different strengths of distortions corresponding to different levels of external influence during the capturing process. This is hardly possible to achieve using real data because one would have to create many different acquisition conditions and ensure stable acquisition conditions during the whole acquisition process across all of the test subjects. In addition, it becomes a tedious and very time-consuming work to establish such datasets for a broad variety of different acquisition conditions in combination with different levels of strength. Finally, it may be impossible to isolate specific external influences from others if there is the need to investigate the impact of a specific type of influence only.

In the following, we describe the StirMark image manipulations which are chosen to be appropriate for finger-vein images and used during the experiments. Not all manipulations provided by StirMark are suitable to simulate natural acquisition conditions. Thus, only a subset of the complete range of image manipulations provided by StirMark is used. For each manipulation, the relation to realistic finger-vein capturing scenarios which could be modelled thereby is outlined. Moreover, the way it is defined is described as well as how it is parametrised to achieve varying strengths. The example images shown have been generated by applying the respective StirMark manipulation.

Median filtering results in a kind of blur to the image, additionally corrupting the clarity of the vein structure. This corresponds to small finger movements during the acquisition of the image (motion blur) or defocus and in general blurry vein structures due to the interaction of the infrared light with different types of tissue inside the finger. The size of the filter mask can be set (height and width of the mask). Figure 9.1(a) shows an example of maximal filter size used.

Remove lines corresponds to errors in finger-vein images resulting either from transmission/processing or errors of the scanner while reading the finger-vein image itself (might not be able to read the entire finger and miss or skip some lines) can be simulated. This manipulation removes lines from the input image the amount of which can be adjusted by a single parameter k which corresponds to the frequency of removing lines, where k means 'remove 1 line in every k lines'.

[3]Currently version 4.0 of the toolkit is available at http: //www.petitcolas.net/fabien/watermarking/stirmark/.

Of course, the output image is reduced in its size while applying this manipulation. An example image with maximal value k can be seen in Figure 9.1(b).

Rotation and cropping corresponds to rotated positioning of the finger on the sensor, with subsequent image cropping to retain image size. Rotation is a very typical, not to say – omnipresent – challenge for finger-vein matching, as in very few cases, a finger will be presented twice in exactly the same orientation to the sensing area during image acquisition. An example image with maximal rotation value used can be seen in Figure 9.2(a).

Embedding watermark Watermarks have been intensively discussed to enhance certain properties of biometric systems [25]. In case robust embedding techniques are being used, impact on recognition accuracy may be expected [26]. StirMark internal watermarks are embedded with increasing strength, resulting in decreasing peak signal-to-noise ration (PSNR). An example image with maximal watermark embedding strength used can be seen in Figure 9.2(b).

Shearing transformation The application of affine transformations to finger-vein images is intended to simulate distortions of the entire finger-vein image, that can appear in real-life situations during acquisition. These distortions depend on the way the finger is positioned in 3-D space relative to the sensor plane. As special cases, we consider *shearing* in both coordinate directions. An example image with

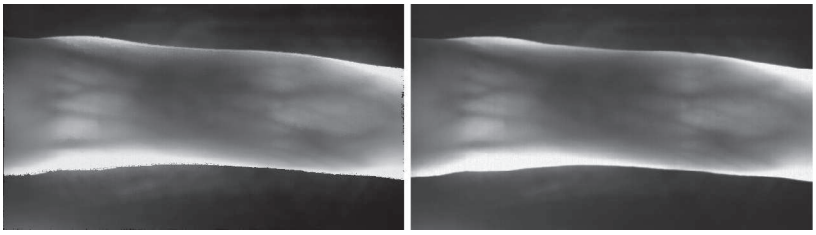

(a) (b)

Figure 9.1 Examples images: (a) median filtering and (b) remove lines

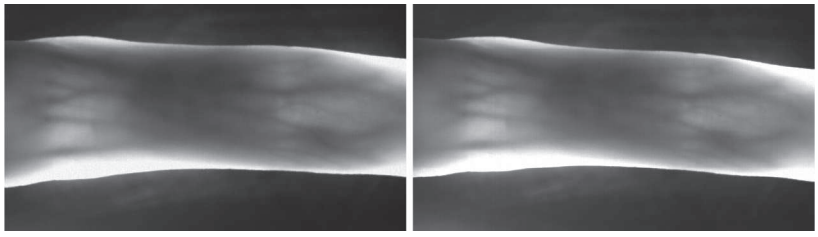

(a) (b)

Figure 9.2 Examples images: (a) rotation and cropping and (b) watermark embedding

maximal shearing strength used can be seen in Figure 9.3(a) where a lesser extent of bending of the finger in *y*-direction can be observed due to the shearing.

Small random distortions These are usually termed *The StirMark Test*. Being a combination of several basic manipulations (i.e. random minor geometric distortion followed by resampling and interpolation, a transfer function to emulate analogue/digital converter imperfections, global 'bending', high frequency displacement, and JPEG compression), this test originally aims to simulate a resampling process, i.e. the errors introduced when printing an image and then scanning it again. The involved image warping is performed both on a global, as well as on a very local level. For the finger-vein scenario, this test can be seen as modelling a very generic, diffuse form of distortion. An example image with maximal strength used can be seen in Figure 9.3(b) where contrasting to most other visual example, the impact of the distortion can easily be observed.

9.3.1 Results

For these experiments, MC feature extraction and matching are used on the UTFVP dataset. As shown in Figures 9.1–9.3, most of the distortions do not affect the subjective quality of the images too much (at least at the resolution possible to use in the display). However, impact on recognition performance can be seen as discussed in the following. In Figure 9.4, we display EER, ZeroFMR (i.e. the lowest FNMR for FMR = 0), as well as ZeroFNMR (i.e. the lowest FMR for FNMR = 0). Please note that polygons not extended until distortion grade 10 indicate that the matching process could not be terminated for these settings (e.g. in the EER plot rotcrop grade > 9).

With respect to EER [Figure 9.4(a)], we notice that shearing (in both directions) affects recognition performance clearly, where shearing in *y*-direction is significantly worse. Also, the removal of entire lines leads to a drastic increase of EER, especially for the higher distortion grades. Also, random distortions clearly affect EER. An interesting effect is observed w.r.t. rotation. While we observe good robustness (only a slight EER increase for grade = 9), the matching software does not work anymore for grade = 10. Obviously, the rotation compensation is no longer able to correct the introduced extent of rotation. Median filtering as well as

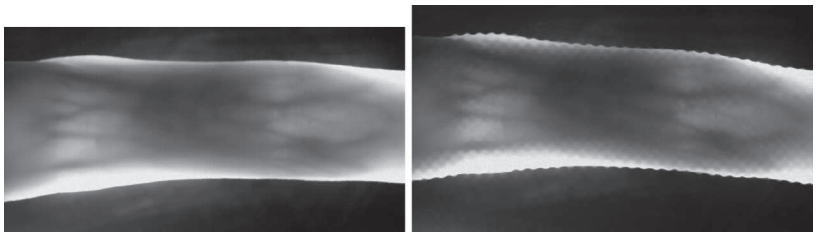

(a) (b)

Figure 9.3 Examples images: (a) shearing in y-direction and (b) small random distortions

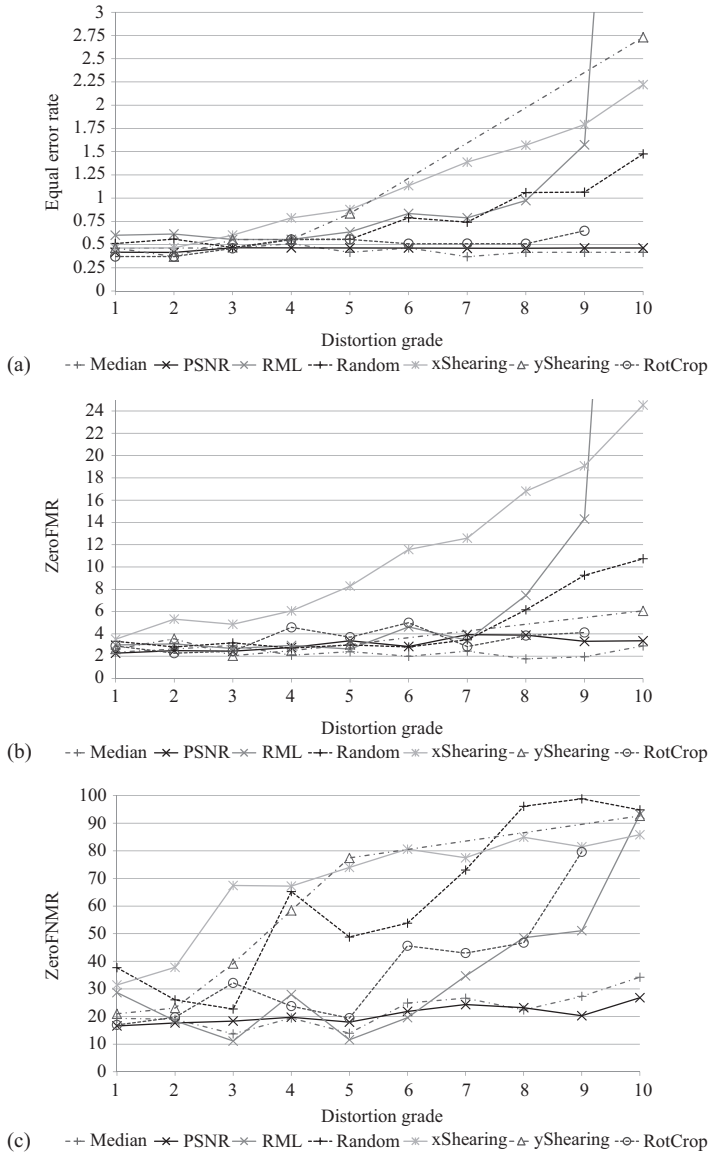

Figure 9.4 Recognition accuracy under StirMark distortions of increasing strengths: (a) EER, (b) ZeroFMR, and (c) ZeroFNMR

watermark insertion does not impact recognition accuracy, at least not up to grade 10. When considering ZeroFMR [Figure 9.4(b)], we observe almost identical relative behaviour of the different distortion types, except for y-shearing which shows less strong impact as compared to EER.

ZeroFNMR as shown in Figure 9.4(c) shows slightly different behaviour. While Median Filtering and Watermark Insertion do not create significantly more false positive matches when increasing their distortion strength, we see small random distortion taking 'the lead' (worst FMR) for high distortion grades and also rotation getting more problematic as observed with EER and ZeroFMR.

Summarising, we may state that different distortion types have a very different impact to MC finger-vein recognition accuracy, and also we have to differentiate between the creation of false positive (higher FMR) or false negative (higher FNMR) matches for different distortion types.

9.4 Compression robustness

Contrasting and in addition to the first and only work on compression robustness of finger-vein recognition [11], we consider an additional non-standardised recent still image compression scheme, we extend the analysis to ZeroFMR (instead of only considering EER), and we consider two datasets (instead of a single one in order to be able to judge generalisation potential of our results). Furthermore, a systematic consideration of compression employment scenarios is conducted.

The certainly most relevant standard for compressing image data relevant in biometric systems is the International Organization for Standardization/International Electrotechnical Commission (ISO/IEC) 19794 standard suite on Biometric Data Interchange Formats where in the most recently published version (ISO/IEC 19794-9:2011 for vascular data), JPEG, JPEG_LS, and JPEG2000 are included for lossy compression (see clause 8.3.13). The ANSI/NIST-ITL 1-2011 standard on 'Data Format for the Interchange of Fingerprint, Facial & Other Biometric Information' (former ANSI/NIST-ITL 1-2007) only supports JPEG2000 for applications tolerating lossy compression.

In this chapter, we consider three different ISO/IEC (lossy) image compression standards and a non-standardised technique for increasing compression rates (i.e. ratio between original file size and file size after compression) up to 110 using the respective default configurations unless stated otherwise:

1. *JPEG (JPG)*: The well-known (ISO/IEC IS 10918-1) Discrete Cosine Transform (DCT)-based image compression method. By adjusting the divisors in the quantisation phase, different compression ratios can be achieved. We adjust the quality parameter iteratively to achieve a file size closest to the desired compression rate. The MATLAB® implementation is used.
2. *JPEG 2000 (J2K)*: The wavelet-based image compression standard (ISO/IEC IS 15444-1) can operate at higher compression ratios as well. J2K is also a part of the Digital Imaging and Communications in Medicine (DICOM) standard where it replaced lossless JPEG compression. Results typically do not generate block-based artefacts as the original DCT-based JPG standard. J2K facilitates explicit rate control, i.e. target bitrates are met with high accuracy. We use JJ2000 version 5.1 available at https://code.google.com/p/jj2000/. For J2K, we additionally employ three variants of region of interest coding (Region of

Interest (ROI), i.e. the pixels corresponding to the finger): first, the classical variant where all the ROI data is coded into the bitstream before the background data; second, where also resolution Level 0 of the background is encoded together with the ROI data; and third, where the first four resolution levels of the background is encoded with the ROI data.

3. *JPEG-XR (JXR)*: This compression standard based on Microsoft's HD Photo is known to produce higher quality than JPEG but provides faster compression than JPEG 2000. In the default configuration, the Photo Overlay/Overlap Transformation is only applied to high pass coefficients prior to the Photo Core Transformation (ISO/IEC IS 29199-2). We adjust quantisation levels iteratively to achieve a target bitrate closest to the desired one. Software available at https://jxrlib.codeplex.com/ is used in experiments.
4. *BPG*: The 'Better Portable Graphics' algorithm is based on a subset of the H.265 (HEVC, ISO/IEC 23008-2) video compression standard. We adjust quantisation levels iteratively to achieve a target bitrate closest to the desired one. The employed software can be downloaded from https://bellard.org/bpg/.

The classical scenario to employ compression in biometric systems is a distributed architecture, where the sensor for authentication sample-data acquisition is dislocated from the biometric matching module. Thus, sample data (the probe) is compressed to facilitate efficient transmission. On the other hand, also enrolment sample data might be kept to enable a change of the template representation without the need for re-enrolment, and if done so, data is certainly compressed (and encrypted) for storage (the gallery). Thus, we have two scenarios how compression may be applied: First, only one sample is compressed (before template generation), i.e. either probe or gallery data (scenario *1-compressed*). And second, both samples involved in matching have been compressed before template extraction (scenario *2-compressed*). Depending on the results we obtain, we may give a recommendation which of the two options should be applied in case we have at least one sample being subjected to compression in mandatory manner (because we may decide if the second sample should be compressed or not depending on the results).

In the experiments, we use both datasets described in Section 9.2, and also the outcome of both recognition schemes (i.e. MC and SIFT) will be compared. Figure 9.5 shows compressed UTFVP images.

It can be clearly seen that JPEG compression is already beyond its limits for sensible operation at a compression ratio of 70 for these type of image data. At compression ratio 110, compression artefacts are clearly visible for JXR and BPG, while J2K subjectively provides the best visual quality.

9.4.1 Results

Subsequent result plots show the compression ratio on the *x*-axis and EER/ZeroFMR on the *y*-axis. We first look into the results of the UTFVP data in the 1-compressed scenario. Figure 9.6 shows a comparison of EER for MC and SIFT recognition on the UTFVP data. It is clearly displayed that JPEG is not competitive for compression ratios >30. Also, BPG is clearly worse compared to JXR and J2K for SIFT recognition.

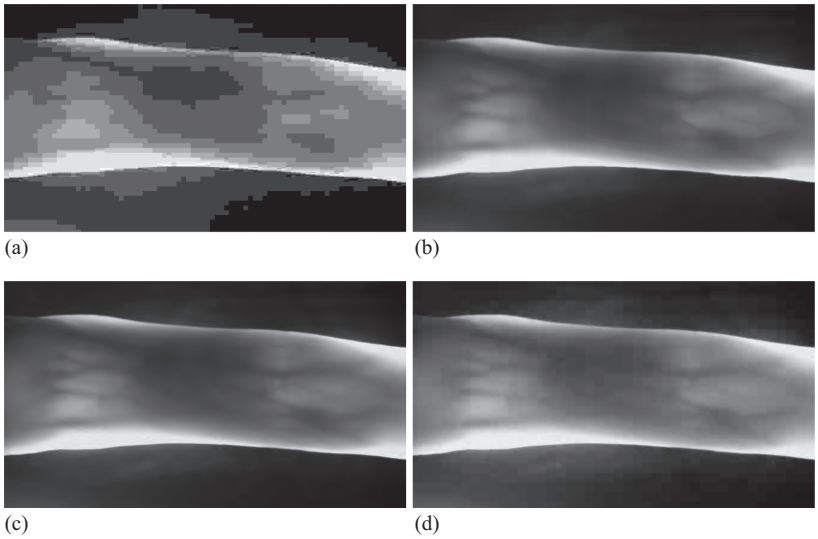

Figure 9.5 Compressed UTFVP images: (a) JPEG, ratio = 70; (b) BPG, ratio = 110; (c) J2K, ratio = 110; and (d) JXR, ratio = 110

More details hidden by the superimposed polygons in Figure 9.6 are shown in Figure 9.7. For MC recognition, the various J2K options are clearly the best, with the 'pure' ROI coding variant being the best option. JXR is clearly inferior, while BPG is the worst option in this detailed view [Figure 9.7(a)]. For SIFT, the different J2K options are pretty close, while JXR is the worst option for most compression ratios.

Figure 9.8 shows results on ZeroFMR. For MC recognition [Figure 9.8(a)], JPEG turns out to lead to very poor results (which are not shown), while the J2K variants are clearly better than BPG and JXR (where again the 'pure' ROI coding is best in most cases). BPG is worst for high compression ratios. For SIFT recognition [Figure 9.8(b)], JPEG and BPG give very poor results, while J2K, J2K ROI, and JXR are rather close in performance.

When comparing the trend for EER and ZeroFMR, we see similar overall trends, while in some details, differences are found: for SIFT, JPEG, and BPG, performance is rather close for ZeroFMR, while in terms of EER BPG is much better. For MC recognition, JXR and BPG exhibit surprisingly good values for compression ratio 70 in terms of ZeroFMR, while this is not visible in terms of EER.

In Figure 9.9, we compare the two scenarios in exemplary plots. Interestingly, in most cases (four out of six), recognition accuracy in terms of EER is superior in the 1-compressed scenario.

When looking more closely to the cases with opposite behaviour, we notice that better results for the 2-compressed scenario are only observed in cases with overall very low EER, i.e. JPEG for high compression ratios (both MC and SIFT

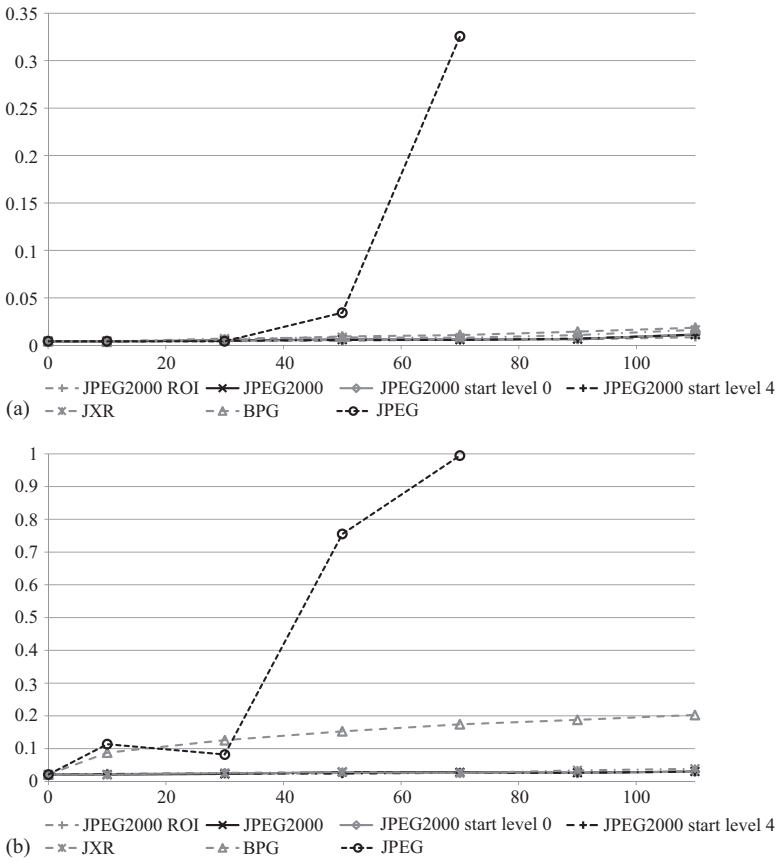

Figure 9.6 Recognition accuracy (EER) under increasing compression strength on UTFVP data (scenario 1-compressed): (a) MC and (b) SIFT

recognition) as well as BPG and SIFT recognition. Thus, under desirable operation conditions, keeping one sample uncompressed is the better option (also saving computational cost for the compression of the second sample).

After the view on isolated single error curves, we additionally provide a comparison of the relation among the error curves of the different compression techniques in Figure 9.10. Figure 9.7(a) (depicting the EER behaviour in scenario 1-compressed) can be directly compared to Figure 9.10(a). While the J2K variants exhibit a very similar behaviour in both scenarios, the superiority of BPG over JXR as seen in scenario 1-compressed can no longer be stated for scenario 2-compressed. The relation of the latter two techniques is actually interchanged when switching scenarios.

By analogy, Figure 9.10(b) displays ZeroFMR behaviour of SIFT recognition in the 2-compressed scenario and can be directly compared to Figure 9.8(b) displaying the 1-compressed case. In this case, we observe very similar relations with

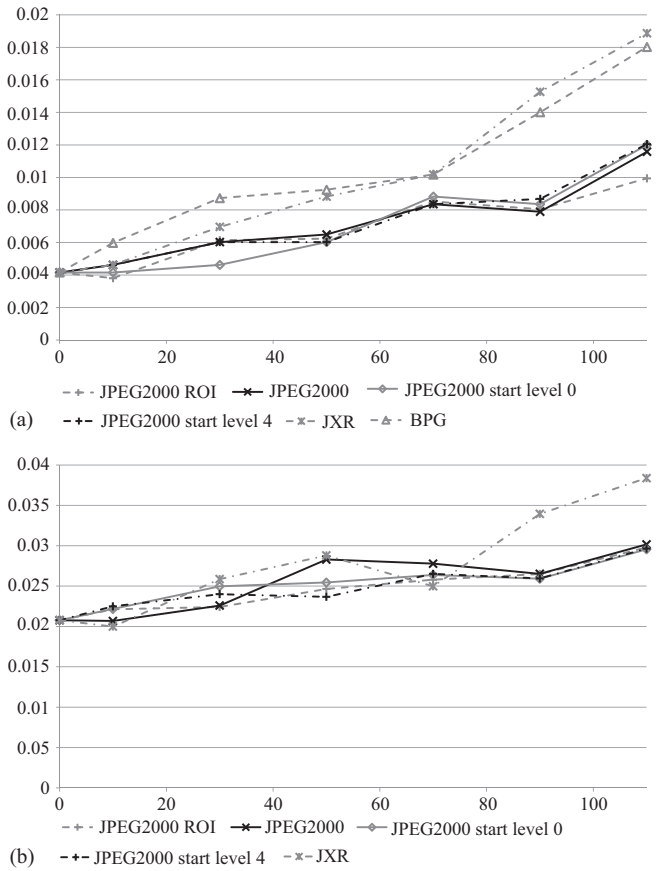

Figure 9.7 Details on recognition accuracy (EER) under increasing compression strength on UTFVP data (scenario 1-compressed): (a) MC and (b) SIFT

the major difference that JXR gets clearly inferior to the J2K variants for higher compression ratios.

In the following, we investigate if the observed results do indeed carry over to the second dataset, i.e. the SDUMLA-HMT data. Again, JPEG results are by far worst, and JPEG is only able to compress the images up to compression ratio 50 (due to the lower resolution of the SDUMLA-HMT data as compared to UTFVP). Figure 9.11 displays EER for the 1-compressed scenario for MC and SIFT recognition, respectively. We again observe for both recognition schemes that the J2K variants are very close and give clearly better behaviour as compared to JXR. BPG behaviour is also quite similar to the UTFVP case – while being close to JXR for MC recognition, the results for SIFT recognition are clearly inferior to J2K and JXR.

ZeroFMR results as shown in Figure 9.12 correspond even better to the expectations. For MC recognition, the clear ranking is identical to the UTFVP data

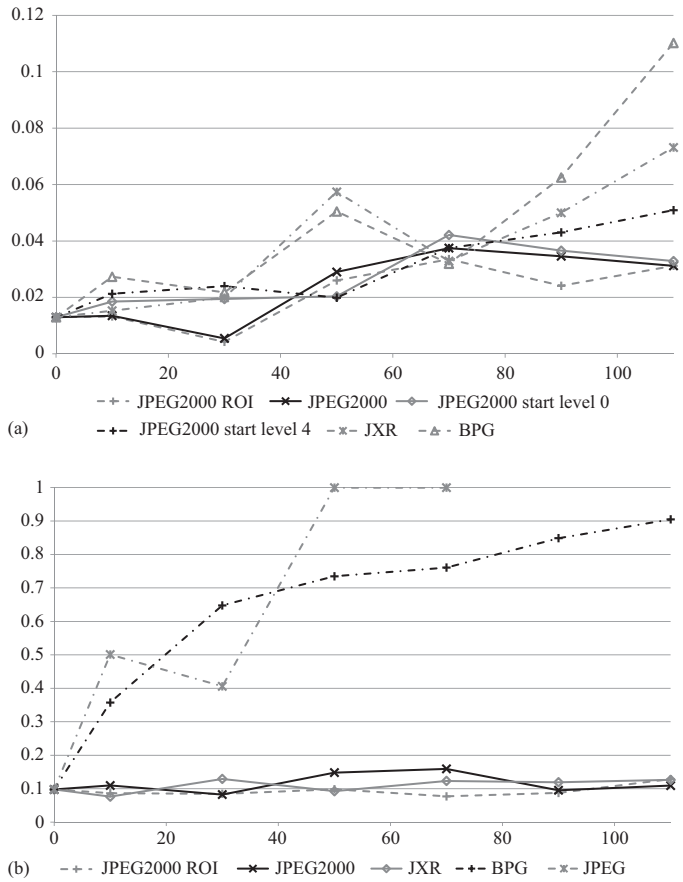

Figure 9.8 Details on recognition accuracy (ZeroFMR) under increasing compression strength on UTFVP data (scenario 1-compressed): (a) MC and (b) SIFT

(i.e. J2K variants best, followed by BPG and JXR), and also the poor BPG results for SIFT recognition do entirely carry over from the UTFVP results.

Overall, results of the two different datasets are in good correspondence. Finally, we aim to verify if the results on comparing 1-compressed to 2-compressed scenario do (also) carry over from the UTFVP data. Thus, in Figure 9.13, we compare the two scenarios in exemplary plots. At first sight, results seem very different from the UTFVP case, as in most cases (four out of six), recognition accuracy in terms of EER is superior in the 2-compressed scenario.

However, when looking at the results more closely, we observe that for the two cases in which scenario 1-compressed is superior, EER behaviour is better as for the other four cases. So overall, again, in the case of good recognition performance, the 1-compressed scenario is advantageous; however, the differences are more subtle as compared to the UTFVP data.

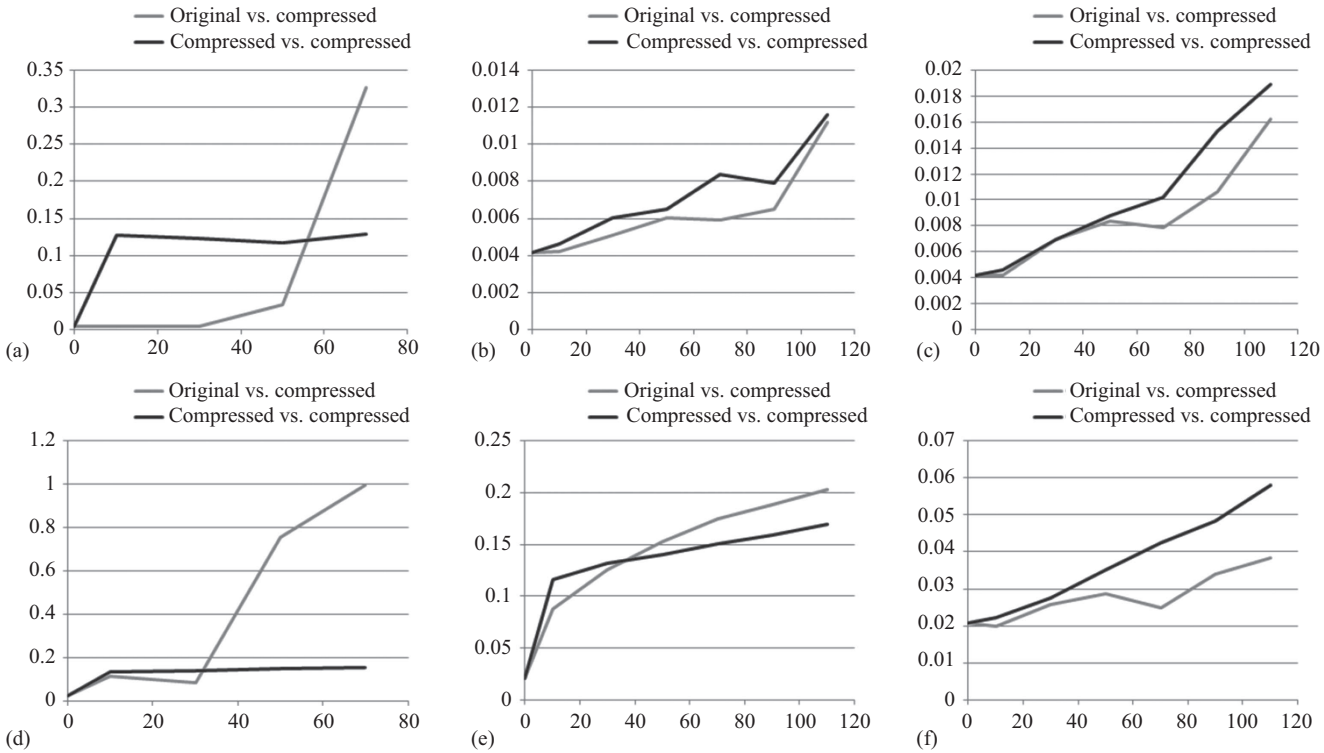

Figure 9.9 Comparing the two scenarios [1-compressed (light grey) vs. 2-compressed (dark grey)] on UTFVP data: (a) JPEG, MC; (b) J2K, MC; (c) JXR, MC; (d) JPEG, SIFT; (e) BPG, SIFT; and (f) JXR, SIFT

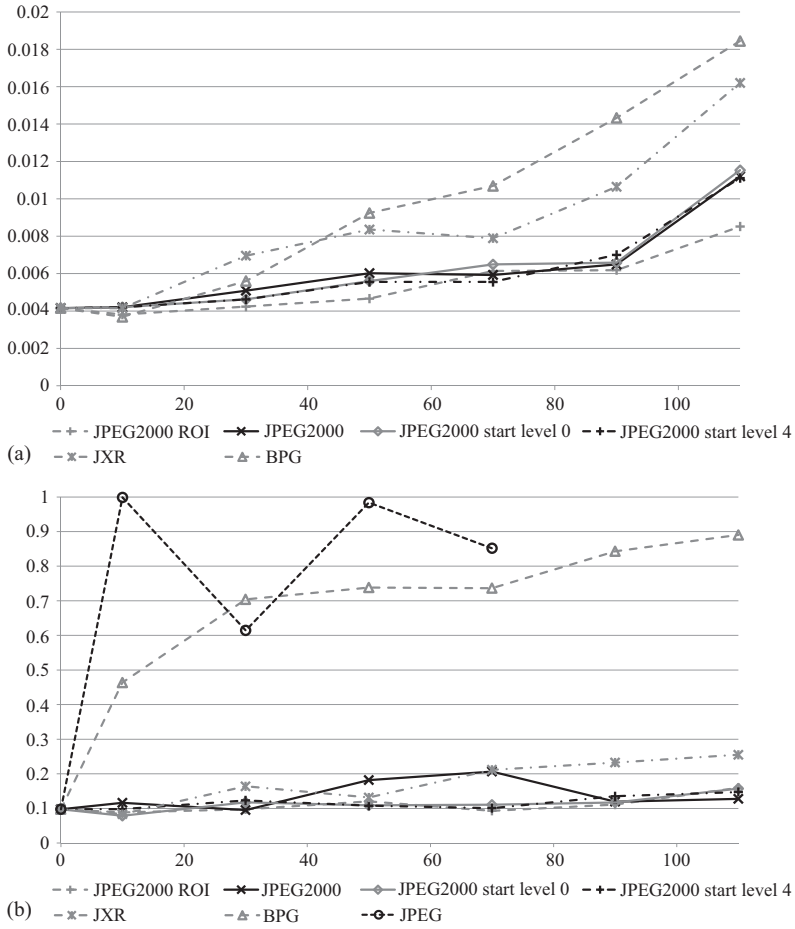

Figure 9.10 Recognition accuracy in the 2-compressed scenario under increasing compression strength on UTFVP data: (a) MC, EER details and (b) SIFT, ZeroFMR

Finally, after the view on isolated single error-curves, we again additionally provide a comparison of the relation among the error curves of the different compression techniques in Figure 9.14. Figure 9.14(a), showing the ZeroFMR with MC recognition in scenario 2-compressed, directly compares to Figure 9.12(a) providing the same data for the 1-compressed scenario. The overall shape of the figures appears to be very similar, but note that the FNMR values for all compression techniques are higher for the 1-compressed scenario. Also, JXR is superior to BPG in the 2-compressed scenario case, which is not true for 1-compressed.

Figure 9.14(b) directly compares to Figure 9.12(b) where we observe very similar behaviour for both scenarios. The only exception is JXR, which is inferior to the J2K variants for a wide range of compression ratios in scenario 2-compressed, but only inferior for the higher ratios in scenario 1-compressed.

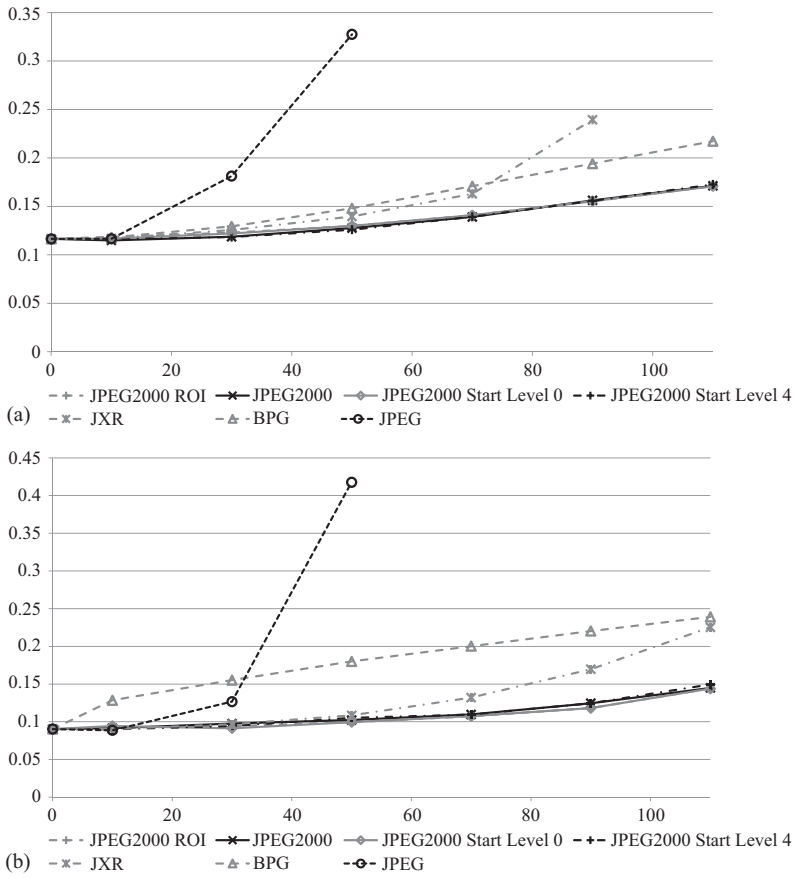

Figure 9.11 Recognition accuracy (EER) under increasing compression strength on SDUMLA-HMT data (scenario 1-compressed): (a) MC and (b) SIFT

9.5 Sensor ageing robustness

Contrasting and in addition to the first and only work on sensor-ageing robustness of finger-vein recognition [10], we consider a different dataset (SDUMLA-HMT instead of UTFVP) to allow to judge generalisation potential of the results and instead of considering EER results only, we also look at the ZeroFMR results to allow more standardised accuracy assessment. To facilitate a fair comparison, we use the identical sensor ageing simulation procedure as in [10] but focusing on the effects of an increasing number of hot and stuck pixels only without looking into combined effects. When being applied to unaltered SDUMLA-HMT data, we find EER for MC recognition to be 0.1045 and ZeroFMR to be equal to 0.2515. For SIFT recognition, we find the EER to be 0.1289, while ZeroFMR is 0.9999.

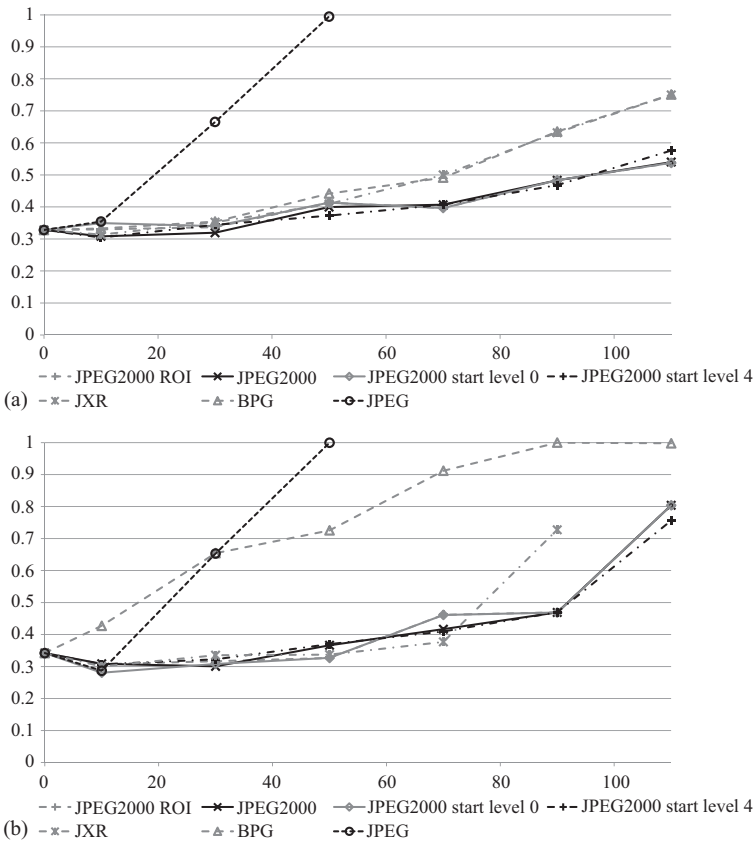

Figure 9.12 Recognition accuracy (ZeroFMR) under increasing compression strength on SDUMLA-HMT data (scenario 1-compressed): (a) MC and (b) SIFT

Thus, comparing EER on unaltered data to the results in [10, Table 2], results for SDUMLA-HMT are significantly worse. In particular, we also note an interesting effect when comparing EER and ZeroFMR: while EER is clearly better for MC on UTFVP as compared to SIFT, on SDUMLA-HMT, the EER exhibits a comparable value for both recognition schemes. Only looking at the ZeroFMR reveals the clearly inferior behaviour of SIFT on this dataset.

9.5.1 Results

The results are evaluated in terms of the absolute EER/ZeroFMR accuracy.

Figure 9.15 displays the results for the SDUMLA-HMT dataset, whereas Figures 1.2 and 1.3 in [10] show the corresponding results for the UTFVP data. Overall, it has to be clearly noted again [10] that under realistic ageing conditions, sensor ageing does not impact finger-vein recognition accuracy.

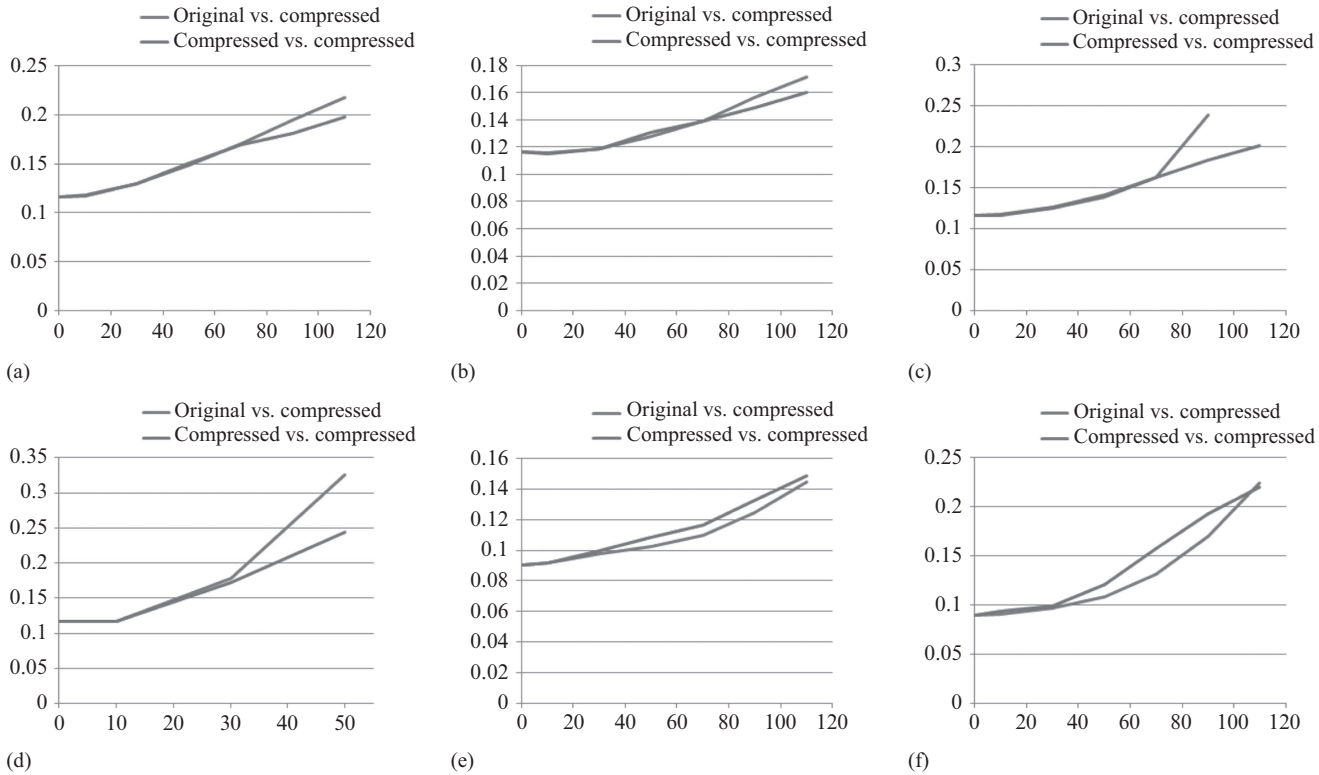

Figure 9.13 Comparing the two scenarios [1-compressed (blue) vs. 2-compressed (red)] on SDUMLA-HMT data: (a) BPG, MC; (b) J2K, MC; (c) JXR, MC; (d) JPEG, SIFT; (e) J2K, SIFT; and (f) JXR, SIFT

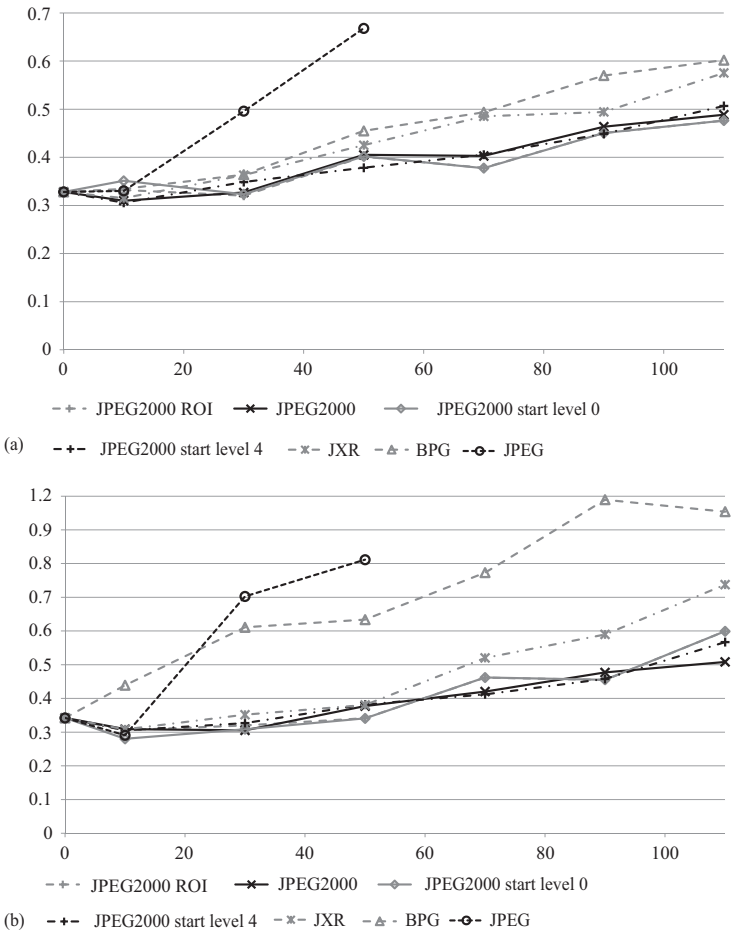

Figure 9.14 Recognition accuracy in the 2-compressed scenario under increasing compression strength on SDUMLA data: (a) MC, ZeroFMR and (b) SIFT, ZeroFMR

However, for high defect rates, interestingly, we notice some differences in the results. For UTFVP data, we do not observe an increase of EER under ageing for hot pixels at all (for both MC and SIFT), and only considering MC we find increasing EER for stuck pixels (EER is constant for SIFT under an increasing number of stuck pixels as well). For SDUMLA-HMT data, different behaviour is seen as follows [Figure 9.15(a)]. For MC recognition, we find increasing EER as long as the number of defects is increased, for both, hot and stuck pixels (for stuck pixels, the situation is worse). For SIFT recognition, EER first increases but then stabilises at values clearly superior to MC in terms of relative difference. Also, the worse behaviour of stuck pixels is only true for a lower number of defects; for higher ones, hot pixels have more impact on SIFT recognition.

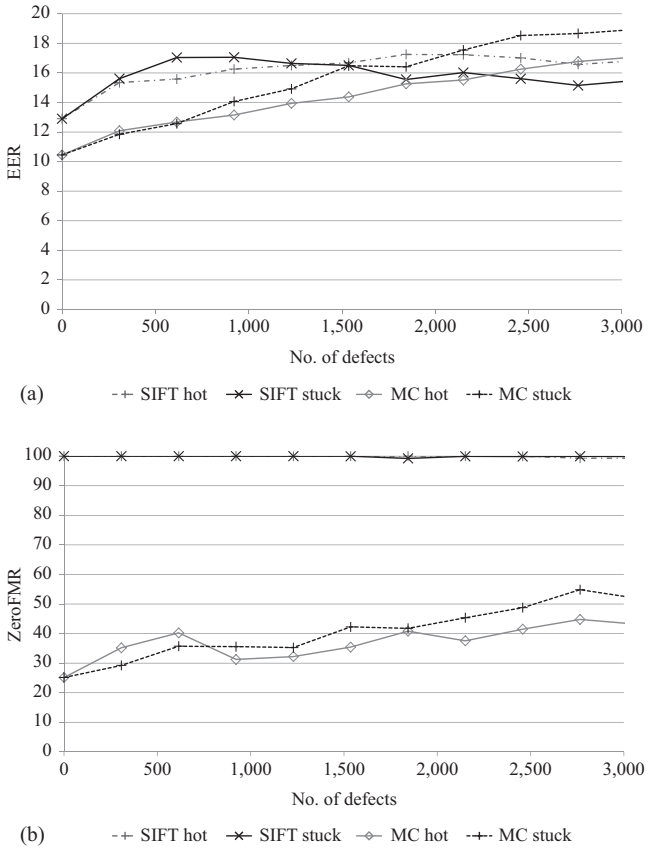

Figure 9.15 Relative recognition accuracy (MC and SIFT algorithms, respectively) under simulated sensor ageing of increasing strength: (a) EER and (b) ZeroFMR

ZeroFMR results, not being considered in [10] [Figure 9.15(b)], do not indicate any change of the SIFT results for an increasing number of defects. This is due to the already catastrophic FNMR values which cannot increase any more. For MC recognition, we find significantly increasing FNMR for increasing defect numbers, more pronounced for stuck pixels at high defect numbers and more pronounced for hot pixels at lower defect numbers.

9.6 Conclusion

For the three different aspects of robustness, we reach the following conclusions:

- **Acquisition conditions:** Incorrect finger placement in 3-D space relative to the sensor plane as modelled by shearing turns out to be highly problematic for recognition performance. Also, an excessive line loss or rotation significantly

impacts on recognition accuracy. On the other hand, it turns out that watermark insertion and median filtering (used to model motion blur or defocus) does not affect finger-vein recognition accuracy too much. It is also interesting to observe that different types of distortions tend to generate different amounts of false positives and false negatives, changing the ranking among distortion types clearly.

- **Lossy compression:** Result correspondence between the two datasets considered is very good; thus, we may assume that our findings also do carry over to other finger-vein data (i.e. sensors). Also, results do carry over from EER-based rankings to ZeroFMR ones; however, differences are more pronounced in some cases for ZeroFMR. With respect to compression scenarios, we have found that in the case of higher recognition accuracy, it is beneficial to have one template being derived from uncompressed sample data, while for situations with lower overall recognition accuracy, it is of advantage to compute both templates involved in matching from compressed data. In terms of compression schemes, JPEG is clearly not useful in medium and high compression ratio settings. On the other hand, JPEG2000 robustly delivers the best performance of all compression schemes; however, the ROI coding option hardly improves over the non-ROI baseline compression technique. Obviously, the image background does not play an important role due to its low information content. BPG, being competitive to the ISO still image compression standards for MC recognition, provides much worse behaviour for SIFT recognition. So it seems that the usefulness of BPG is highly dependent on the used recognition scheme.
- **Sensor ageing**: In usual sensor operation conditions, sensor ageing does not pose a problem for finger-vein recognition accuracy. However, when increasing sensor defects to surpass 'natural' levels, we find partially significant dataset dependencies in the results. Thus, we recommend to experimentally identify the most appropriate feature extraction and pre-processing schemes given specific data sets and ageing conditions.

Acknowledgements

We acknowledge and highly appreciate the dedicated work of the students Christian Barthel, Tamara Lipowski, Babak Maser, Simone Oblasser, and Elaheh Yousefiamiri for generating experimental data for this chapter in the context of the Media Data Formats Lab at the University of Salzburg.

References

[1] F. Alonso-Fernandes, J. Bigun, J. Fierrez, H. Fronthaler, K. Kollreider, and J. Ortega-Garcia. Fingerprint recognition. In D. Petrovska-Delacretaz, G. Chollet, and B. Dorizzi, editors, *Guide to Biometric Reference Systems and Performance Evaluation*, pages 51–88. Springer-Verlag, 2009.

[2] D. Maltoni, D. Maio, A. K. Jain, and S. Prabhakar. *Handbook of Fingerprint Recognition* (*2nd Edition*). Springer-Verlag, 2009.

[3] A. Noviyanto and R. Pulungan. A comparison framework for fingerprint recognition methods. In *Proceedings of the 6th SEAMS-UGM Conference (Computer, Graph and Combinatorics)*, pages 601–614, 2011.

[4] R. Cappelli. Synthetic fingerprint generation. In D. Maltoni, D. Maio, A.K. Jain, and S. Prabhakar, editors, *Handbook of Fingerprint Recognition* (*2nd Edition*), pages 271–302. Springer-Verlag, 2009.

[5] M. Kutter and F. A. P. Petitcolas. Fair evaluation methods for image watermarking systems. *Journal of Electronic Imaging*, 9(4):445–455, October 2000.

[6] J. Hämmerle-Uhl, M. Pober, and A. Uhl. Towards standardised fingerprint matching robustness assessment: The stirmark toolkit – cross-feature type comparisons. In *Proceedings of the 14th IFIP International Conference on Communications and Multimedia Security (CMS'13)*, volume 8099 of *Springer Lecture Notes on Computer Science*, pages 3–17, Magdeburg, Germany, September 2013.

[7] J. Hämmerle-Uhl, M. Pober, and A. Uhl. Towards standardised fingerprint matching robustness assessment: The stirmark toolkit – cross-database comparisons with minutiae-based matching. In *Proceedings of the 1st ACM Workshop on Information Hiding and Multimedia Security (IH&MMSec'13)*, pages 111–116, Montpellier, France, June 2013.

[8] C. Kauba and A. Uhl. Fingerprint recognition under the influence of sensor ageing. In *Proceedings of the 4th International Workshop on Biometrics and Forensics (IWBF'16)*, pages 1–6, Limassol, Cyprus, 2016.

[9] C. Kauba and A. Uhl. Robustness evaluation of hand vein recognition systems. In *Proceedings of the International Conference of the Biometrics Special Interest Group (BIOSIG'15)*, pages 1–8, Darmstadt, Germany, 2015.

[10] C. Kauba and A. Uhl. Sensor ageing impact on finger-vein recognition. In *Proceedings of the 8th IAPR/IEEE International Conference on Biometrics (ICB'15)*, pages 1–8, Phuket, Thailand, May 2015.

[11] V. Ablinger, C. Zenz, J. Hämmerle-Uhl, and A. Uhl. Compression standards in fingervein recognition. In *Proceedings of the 9th IAPR/IEEE International Conference on Biometrics (ICB'16)*, pages 1–7, 2016.

[12] E. C. Lee, H. C. Lee, and K. R. Park. Finger vein recognition using minutia-based alignment and local binary pattern-based feature extraction. *International Journal of Imaging Systems and Technology*, 19(3):179–186, 2009.

[13] B. Huang, Y. Dai, R. Li, D. Tang, and W. Li. Finger-vein authentication based on wide line detector and pattern normalization. In *Pattern Recognition (ICPR), 2010 20th International Conference on*, pages 1269–1272. IEEE, 2010.

[14] K. Zuiderveld. Contrast limited adaptive histogram equalization. In P. S. Heckbert, editor, *Graphics Gems IV*, pages 474–485. Morgan Kaufmann, 1994.

[15] J. Zhao, H. Tian, W. Xu, and X. Li. A new approach to hand vein image enhancement. In *Intelligent Computation Technology and Automation, 2009.*

ICICTA'09. Second International Conference on, volume 1, pages 499–501. IEEE, 2009.

[16] J. Zhang and J. Yang. Finger-vein image enhancement based on combination of gray-level grouping and circular gabor filter. In *Information Engineering and Computer Science, 2009. ICIECS 2009. International Conference on*, pages 1–4. IEEE, 2009.

[17] N. Miura, A. Nagasaka, and T. Miyatake. Extraction of finger-vein patterns using maximum curvature points in image profiles. *IEICE Transactions on Information and Systems*, 90(8):1185–1194, 2007.

[18] N. Miura, A. Nagasaka, and T. Miyatake. Feature extraction of finger-vein patterns based on repeated line tracking and its application to personal identification. *Machine Vision and Applications*, 15(4):194–203, 2004.

[19] D. G. Lowe. Object recognition from local scale-invariant features. In *Proceedings of the Seventh IEEE International Conference on Computer Vision (CVPR'99)*, volume 2, pages 1150–1157. IEEE, 1999.

[20] C. Kauba, J. Reissig, and A. Uhl. Pre-processing cascades and fusion in finger vein recognition. In *Proceedings of the International Conference of the Biometrics Special Interest Group (BIOSIG'14)*, Darmstadt, Germany, September 2014.

[21] B. T. Ton and R. N. J. Veldhuis. A high quality finger vascular pattern dataset collected using a custom designed capturing device. In *International Conference on Biometrics, ICB 2013*. IEEE, 2013.

[22] Y. Yin, L. Liu, and X. Sun. SDUMLA-HMT: A multimodal biometric database. In *The 6th Chinese Conference on Biometric Recognition (CCBR 2011)*, volume 7098 of *Springer Lecture Notes on Computer Science*, pages 260–268, 2011.

[23] D. Maio, D. Maltoni, R. Cappelli, J. L. Wayman, and A. K. Jain. FVC2004: Third fingerprint verification competition. In *ICBA, volume 3072 of LNCS*, pages 1–7. Springer Verlag, 2004.

[24] F. A. P. Petitcolas, R. J. Anderson, and M. G. Kuhn. Attacks on copyright marking systems. In D. Aucsmith, editor, *Information Hiding: Second International Workshop*, volume 1525 of *Lecture Notes in Computer Science*, pages 218–238, Portland, OR, USA, April 1998. Springer Verlag, Berlin, Germany.

[25] J. Hämmerle-Uhl, K. Raab, and A. Uhl. Watermarking as a means to enhance biometric systems: A critical survey. In T. Filler, T. Pevny, S. Craver, and A. Ker, editors, *Proceedings of the 2011 Information Hiding Conference (IH'11)*, volume 6958 of Springer LNCS, pages 238–254, Prague, Czech Republic, 2011.

[26] J. Hämmerle-Uhl, K. Raab, and A. Uhl. Experimental study on the impact of robust watermarking on iris recognition accuracy (best paper award, applications track). In *Proceedings of the 25th ACM Symposium on Applied Computing*, pages 1479–1484, 2010.